Materials Chemistry and Physics 205 (2018) 494–501

Contents lists available at ScienceDirect

Materials Chemistry and Physics

journal homepage: www.elsevier.com/locate/matchemphys

Amorphous Ni-C nanoparticles with high electric conductivity and high specific capacitance for rechargeable charge storage

Yu-Mei Hu [a], Yu-Xia Hu [c], Mao-Cheng Liu [a, b, *], Jia-Jia Li [a], Ling-Bin Kong [b], Yong-Chun Luo [b], Long Kang [b]

[a] State Key Laboratory of Advanced Processing and Recycling of Non-ferrous Metals, Lanzhou University of Technology, Lanzhou 730050, PR China
[b] School of Materials Science and Engineering, Lanzhou University of Technology, Lanzhou 730050, PR China
[c] School of Bailie Engineering and Technology, Lanzhou City University, Lanzhou 730070, PR China

HIGHLIGHTS

- Amorphous Ni-C with high conductivity has been fabricated for supercapacitors.
- Ultrahigh specific capacitance with superior cycling stability has been achieved.
- Ni-C//AC is assembled and delivered high energy density and long lifespan.

GRAPHICAL ABSTRACT

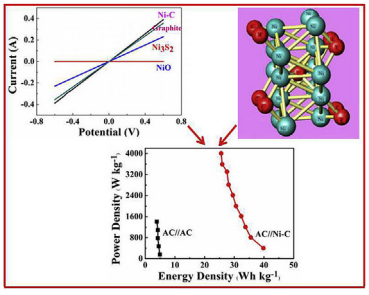

ARTICLE INFO

Article history:
Received 27 June 2016
Received in revised form
3 October 2017
Accepted 13 November 2017
Available online 14 November 2017

Keywords:
Amorphous materials
Carbides
Electrical conductivity
Electrochemical properties

ABSTRACT

High electrical conductivity is a crucial factor for improving the electrochemical performance of energy storage materials. In the work, amorphous Ni-C nanoparticles with high electric conductivity are fabricated by mechanical alloying and are used as a novel cathode for supercapacitors. It is shown that the amorphous Ni-C retains a high specific capacitance and remarkable cycling stability after the electrode is activated by chronopotentiometry at 0.5 A g^{-1}, and even more gratifyingly, the rate capability of the material is superior to that of other Ni based materials due to its high electrical conductivity, which is convenient for fast electron transfer in active material and fast reversible Faradic reaction characteristics. Finally, an asymmetric supercapacitor based on Ni-C as the positive electrode and activated carbon as the negative electrode could be cycled reversibly at a high working potential of 0–1.6 V and delivered a high energy density of 39.8 Wh kg^{-1}. These results confirm the significance and tremendous potential of amorphous Ni-C materials for the development of high-performance energy supply systems.

1. Introduction

Due to the ongoing depletion of fossil energy resources and serious environmental pollution, the development of new clean energy has become inevitable for the sustainable development of human society [1–3]. However, the utilization of these clean energy resources in industry and daily life requires the use of energy

* Corresponding author. State Key Laboratory of Advanced Processing and Recycling of Non-ferrous Metals, Lanzhou University of Technology, Lanzhou 730050, PR China.
E-mail address: liumc@lut.cn (M.-C. Liu).

https://doi.org/10.1016/j.matchemphys.2017.11.032
0254-0584/

storage devices, with the traditional storage devices including Ni-MH batteries, lithium-ion batteries, and fuel cells [4–6]. Unfortunately, these energy storage devices have not been able to meet the energy needs in applications such as departure gate, laptop computers, and autonomous microsystems for the development of wireless sensing due to either a low power density or longer charge and discharge time; thus, an energy storage device that not only has a high energy density but also has a high power density as well as a short charge and discharge time is urgently required. Therefore, a new type of energy storage device has been developed, namely, the supercapacitor, which has recently been studied extensively because of its high energy density, high power density, short charge time, good safety, and long cycle life [7–10]. Since it is known that electrode characteristics are important for the performance of supercapacitors, it is necessary to search for high-performance electroactive electrodes to further enhance the energy density of supercapacitors [11,12].

Carbon materials are the earliest used electrode material, which store energy by the confrontation of opposite sign charges in the electrode/electrolyte interphase and such ECs are known as electrochemical double-layer capacitors (EDLCs), the specific capacitance of EDLCs in the aqueous electrolyte measured to be less than 250 F g^{-1} [13–15]. To overcome this limitation, the vast majority of researchers that are currently working on ECs have focused on improving the specific capacitance, and pseudocapacitors using surface redox pseudo-capacitive materials have been developed [16–19]. Over the past few decades, a tremendous amount of work on pseudo-capacitive materials has been performed on Ni-based materials due to their high specific capacitance. For example, NiO nanoparticles on different substrates were successfully synthesized and displayed a high specific capacitance of 1386 F g^{-1} [20], Cao et al. showed that NiO can exhibit the capacitance of 675 F g^{-1} at 2 A g^{-1} [21], Guan et al. also recorded 196.5 mAh g^{-1} for NiO in KOH electrolyte [22], Yang et al. fabricated NiS-based capacitors that showed a capacitance of 905.3 F g^{-1} at a current density of 0.5 A g^{-1} [23], Yu et al. successfully synthesized Ni_3N/graphene nanocomposites and demonstrated a high specific capacitance of 2087.5 F g^{-1} at 1 A g^{-1} [24], and Zhang et al. showed that Ni_3S_2 exhibits a capacitance of 710.4 F g^{-1} in alkaline electrolyte [25]. Although all of these nickel-based materials exhibited high specific capacitance values, their rate performance is poor and few studies have explored the electrical conductivity of these materials. Electrical conductivity is the reciprocal of resistivity, and represents the ability of the material to transfer a current, and a material with a high electrical conductivity will show excellent rate performance at high current charge discharge. Therefore, the synthesis of other nickel-based compounds with high conductivity, not only can yield a high specific capacitance, but can also significantly improve the rate performance. Metal carbides, also called cermets, have been shown to display many advantages, such as: a) excellent electrical conductivity (4000–55500 S cm^{-1}) that is much higher than that of nickel oxide and b) substantially larger specific capacitance than carbon materials that can give rise to high energy density [26]. Some metal carbides have recently been used in supercapacitors, especially titanium carbide, such as in the work of Ghidiu et al. and Naguib et al. who recently synthesized titanium carbide-based supercapacitors [27,28]. However, the low specific capacitance makes it difficult to apply these materials in practical use, and the preparation method is not only cumbersome, but can also cause pollution. Therefore, it is especially important to choose a simple preparation method for use in production. The method of mechanical alloying is an effective method for the preparation of high-melting-point compounds such as metal carbides or metal sulfides. In the milling process, the material will change to the amorphous phase, and many experimental results show that this phase displays better electrochemical performance than the crystal phase [29,30].

Herein, an amorphous Ni-C electrode with high electrical conductivity has been successful synthesized by a facile mechanical alloying method and is found to exhibit a specific capacitance of 1000 F g^{-1} at 0.5 A g^{-1} after the electrode is activated by the consecutive current charge-discharge curve in 6 M KOH. To evaluate performance of the amorphous Ni-C electrode in practical applications, an asymmetric supercapacitor (named AC//Ni-C) was assembled. The supercapacitor displays a high specific capacitance and an outstanding cycle stability. These results demonstrate the potential application value of amorphous Ni-C materials for the continuing development of energy storage systems.

2. Experimental section

Nickel powder (99.9%, 325–400 mesh) and acetylene black (AR) were purchased from Beijing Puruixincai Technology Co. Ltd. and the Hunan Zhengyuan Institute of Energy Storage Materials and Devices, respectively. To reduce the contact resistance between the active substance and the current collector, nickel foam was treated prior to use in this experiment, according to the following procedure: first, a piece of foam nickel was cut into a rectangular shape with the dimensions of 1 cm × 2.5 cm, and then the foam nickel was cleaned by the ethanol and acetone several times to remove the oily layer and the surface oxide layer.

Amorphous Ni-C was fabricated by mechanical alloying as follows. Ni and acetylene black powders were placed in a jar together with stainless steel balls. The weight ratio of steel balls to powder was 15:1. The stainless steel balls were fit together in an argon-filled glove box and ball milling (Spex-8000) was conducted under an Ar atmosphere.

3. Electrochemical measurements

The preparation process of the electrodes is detailed in our previous article [29]. The structure characterization equipments and the preparation progress of the asymmetric supercapacitor are shown in supporting information.

3.1. Structure characterization

The structure of the amorphous Ni-C was characterized by X-ray diffraction (XRD) using a Rigaku D/MAX 2400 diffractometer (Japan) with Cu Kα radiation (λ = 1.5418 Å) operating at 40 kV and 60 mA. In addition, the composition of the surface of the as-synthesized sample was investigated by X-ray photoelectron spectroscopy (XPS, ESCALAB 250, Thermo VG). Raman spectra were obtained using a laser micro-Raman spectrometer (Renishaw InVia) employing a visible laser (514.5 nm) with an output laser power of 40 mW at the excitation wavelength at room temperature. The morphology and particle size were measured by field emission scanning electron microscopy (SEM, JEOL, JSM-6701F, Japan). Transmission electron microscopy (TEM, JEOL, JEM-2010, Japan) was carried out at 200 kV.

3.2. Preparation of the electrode

The electrodes were prepared by coating electrode slurries (80 wt% active material, 7.5 wt% carbon black, 7.5 wt% conducting graphite and 5 wt% of polytetrafluoroethylene with a few drops of ethanol) on an open-cell nickel foam and pressing at 10 MPa, followed by drying at 60 °C for 12 h. Each electrode contained 4 mg of the electroactive material and had a geometric surface area of 1 cm^2. In the current-voltage (I–V) tests, the sample (150 mg) was

crushed into a wafer in a mold to produce three wafers from three samples with uniform diameters (~1 cm) and thicknesses (~2 mm); then, the wafer was placed in the middle of two stainless steel sheets and tested in the electrochemical work station.

3.3. Electrochemical measurements

Electrochemical measurements were performed on a Chen-hua CHI660D workstation in three-electrode mode fitted with a working electrode, a platinum foil counter electrode, and a saturated calomel reference electrode (SCE). Cyclic voltammetry (CV), galvanostatic charging and discharging (GCD) tests, electrochemical impedance spectroscopy (EIS) and cyclic stability studies were performed to investigate the electrochemical behavior of the amorphous Ni-C electrode before and after electrochemical activation.

3.4. Preparation of the asymmetric supercapacitor

The asymmetric supercapacitor consisted of two electrically isolated electrodes: Ni-C as the positive electrode and AC as the negative electrode, with 80 wt% of the active material mixed with 7.5 wt% acetylene black and 7.5 wt% conducting graphite in an agate mortar until a homogeneous black powder was obtained. To this mixture, 5 wt% of polytetrafluoroethylene (PTFE) was added together with a few drops of ethanol. The resulting paste was pressed at 10 MPa into a nickel foam and was then dried at 80 °C for 12 h and joined together by a porous non-woven cloth separator soaked in 6 mol L^{-1} aqueous KOH solution. Each electrode had a geometric surface area of 1 cm^2. For a supercapacitor, the charge balance follows the relationship:

$$Q_+ = Q_- \tag{1}$$

where Q_+ and Q_- represent the charges stored in the positive and negative electrodes, respectively. The Q of each electrode depends on the specific capacitance (C_m), the potential range of the charge/discharge tests (ΔE), and the mass of the electrode (m) according to the following equation:

$$Q = C_m \cdot m \cdot \Delta E. \tag{2}$$

For $Q_+ = Q_-$, the ratio of the masses of the positive electrode (m_+) and negative electrode (m_-) is given by:

$$\frac{m_+}{m_-} = \frac{C_{-m}}{C_{+m}} \cdot \frac{\Delta E_-}{\Delta E_+}. \tag{3}$$

4. Results and discussion

4.1. Structural analysis

The XRD results of the amorphous Ni-C electrode before and after electrochemical activation are presented in Fig. 1a. It can be seen that not only the electrode before activation but also after activation exhibits an amorphous state. This means that there is no change in the amorphous state during the electrochemical activation process, which illustrates that the amorphous structure can be maintained in the electrode reaction process. This is advantageous for preventing the capacity attenuation due to the change of the structure during the reaction. To further explore the composition of the amorphous Ni-C electrode, the X-ray photoelectron spectroscopy (XPS) technique was performed to determine the binding energy and the valence state, with the typical XPS survey scan spectra of the Ni-C before and after activation shown in Fig. 1b. The two figures show the existence of nickel peaks, carbon peaks, and oxygen peaks (the O peaks can be derived from the physical adsorbed from the atmosphere), representing the major components in the sample surface. The high-resolution (HR) Ni 2p XPS

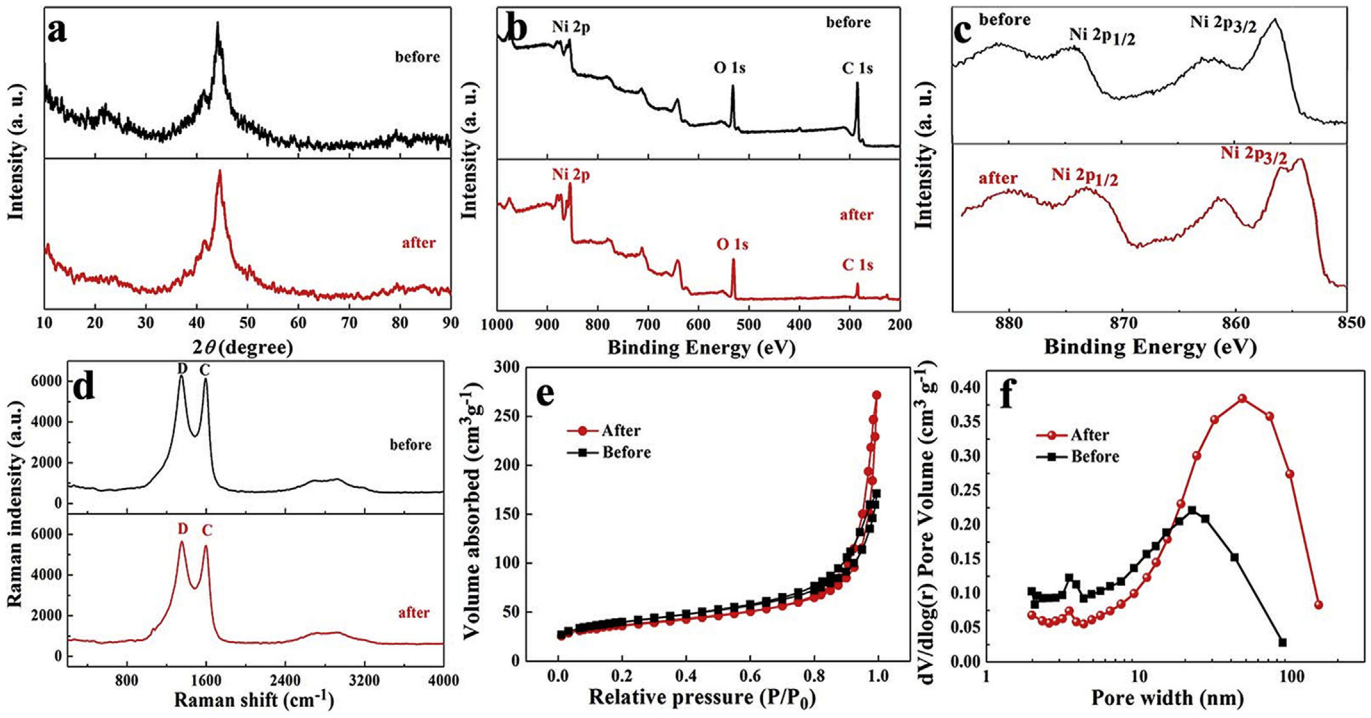

Fig. 1. The Ni-C before and after electrochemical activation (a) XRD patterns, (b) the overall XPS spectrum, (c) XPS Ni2p spectrum, (d) Raman spectrum, (e) the N_2 adsorption–desorption isotherm curve, (f) pore-size distribution.

spectrum for amorphous Ni-C material before and after activation is exhibited in Fig. 1c, with the binding energies for Ni $2p_{3/2}$ and Ni $2p_{1/2}$ are found at 857.68 eV and 875.68 eV, respectively, indicating the Ni^{2+} state [25,31]. Similarly, the binding energies at 857.28 eV and 875.58 eV are assigned to the Ni $2p_{3/2}$ and Ni $2p_{1/2}$ of the Ni^{2+} state for the activated sample, and the peak appearing at 853.78 eV is assigned to the Ni $2p_{3/2}$ of Ni, Therefore, both elemental Ni and Ni^{2+} exist in the active Ni-C surface because both covalent bonds and metal bonds are present in Ni-C, the metal bond in the Ni-C providing a large number of free electrons so that Ni-C has a high conductivity similar to that of a metal. The Raman spectrum of the Ni-C electrode before and after activation are shown in Fig. 1d. It can be seen that the peaks at approximately 1593 cm^{-1} and 1350 cm^{-1} appear for the prepared Ni-C, indicating that the raw material was converted to the amorphous state. In addition, the wide Raman peak appearing at 2750 cm^{-1} is assigned to the G′ band, which is a typical characteristic of amorphous carbon [32]. Surprisingly, the Raman spectra of the activated sample was almost unchanged, which indicates that the sample is still amorphous after activation and fully maintained its structure. Fig. 1e and f show the Nitrogen adsorption/desorption curve of activated Ni-C and the pore size distribution (PSD) of the Ni-C electrode before and after activation. The observed hysteresis type behavior suggests that the Ni-C before and after activation shows hierarchical porous properties with the calculated specific surface areas of 135.23 $m^2\ g^{-1}$ and 129.59 $m^2\ g^{-1}$, respectively. Because the particles of amorphous materials are usually smaller than those of crystalline materials, the specific surface area is much higher than many crystalline materials prepared by mechanical alloying. The pore-size distribution (Fig. 1f) was determined from the desorption branch of the isotherm using the Barrett–Joyner–Halenda (BJH) method. It is obvious that the main pore-size distribution ranging from mesopore to macroporous, the average pore size is 9.69 nm and 17.8 nm. As we know, this type of porous structure can provide more surface active sites and make reactants transport easier [33,34], reduce electron-transport and ion-transport pathways, resulting in high specific capacitance.

The results of morphology characterizations of the Ni-C electrode before and after electrochemical activation are shown in Fig. 2. It can be observed from Fig. 2 (a, b) that the Ni-C electrode before electrochemical activation shows irregular shapes of approximately 70–150 nm in diameter and the particles are attached to each other, providing a stable morphology structure for the continuous electrochemical reaction. The differences in the brightness in the TEM image (Fig. 2c) further confirms that the particles are attached to each other. Simultaneously, the structural characteristics of the Ni-C particles was also studied by EDS mapping with the results shown in Fig. 2(d-f); as seen from the element distribution, Ni and C are distributed uniformly among all the Ni-C particles, which can be explained by the C uniformly distributing in the Ni, and the amorphous Ni-C is ultimately formed. Fig. 2(g and h) show the SEM images of the Ni-C electrode after electrochemical activation, and it can be seen that the particles still show gathered granule morphology, that is to say that the shape of the sample after the reaction has not changed fundamentally, further proving that the material has excellent structural stability. A TEM image of an amorphous Ni-C nanoparticle is shown in Fig. 2i. This morphology could be further observed from the EDS mapping images presented in Fig. 2(j-l). Structural stability of electrode materials is required to maintain a long cycle life and is therefore highly important; it can be seen that no changes in the structure and physical Ni-C phase have occurred after electrochemical activation, indicating that Ni-C structure and physical phase can be retained in the electrode reaction process, avoiding the capacity attenuation caused by structural damage and phase transition, this is advantageous for improving the cycle life.

4.2. Electrochemical measurements

The optimal sample selection process is shown in Fig. S1, and it can be seen that the largest specific capacitance was found for the sample obtained using a milling time of 8 h and a rate of 450 rpm. Fig. 3a and d show that all CV profiles exhibit a few strong redox peaks at all scan speeds. This shows that amorphous Ni-C before and after activation shows typical Faradaic behavior, with the redox peak currents increasing with increased scanning speed. This is, because at increased scanning speed, the surface concentration of reaction components changes faster, further giving rise to the spread of the components in less than the scanning time, this phenomenon can also be confirmed by using $i_p = (2.69*10^5)n^{3/2}AD_0^{1/2}C_0^*v^{1/2}$(where i_p is the anodic peak current, n is the number of the electrons involved in the electrode reaction, A is the area, D_0 is the diffusion coefficient, C_0^* is the concentration, v is the scan rate) [30], the data for the anodic peak current and the square root of scan rate are shown in Fig. S2. Fig. 3b and e show the galvanostatic charge–discharge curves of the Ni-C electrode before and after electrochemical activation. Using the equations for the specific capacitance ($C_m = \frac{C}{m} = \frac{I \cdot \Delta t}{m \cdot \Delta V}$), the highest specific capacitance (C_m) values of the Ni-C electrode before and after electrochemical activation were calculated to be 407.5 F g^{-1} and 1000 F g^{-1}. Additionally, the C_m for Ni-C electrode before and after electrochemical activation as a function of current densities are presented in Fig. 3c and f. For the Ni-C electrode before electrochemical activation, approximately 68.7% specific capacitance retention is observed from 0.5 A g^{-1} to 8 A g^{-1}, whereas for the Ni-C electrode after electrochemical activation, there is around 58% specific capacitance retention from the current density of 0.5–8 A g^{-1} is observed. This indicates that while the electrode improves the specific capacitance immensely after electrochemical activation, but the rate performance is decreased, Even so, the obtained electrode still shows better than some previously reported nickel based materials, such as $Ni(OH)_2$, NiO, Ni_3S_2 and Ni_3Si_2 [35–38]. All of these excellent electrochemical performances of the Ni-C electrode prove its potential for use in energy storage devices.

Electrical conductivity affects the properties of supercapacitor electrode because the material with a high conductivity will provide a high number of electrons for fast surface redox reactions. The current-voltage (I-V) curves of the Ni-C, Ni_3S_2, commercial NiO, and commercial graphite materials tested by linear sweep voltammetry are shown in Fig. 4. It can be seen from the figure that the electrical conductivity of the Ni-C is significantly higher than that of Ni_3S_2, commercial NiO and commercial graphite because the slope of the curve is proportional to the electrical conductivity and the slope for the Ni-C data is higher than those for the Ni_3S_2 and commercial NiO. This is mainly due to the existence of metallic bonds in the Ni-C structure, the high electrical conductivity is beneficial for fast electron transfer of electrode materials at high-rate, and it therefore can significantly improve the rate performance.

The electrochemical impedance spectroscopy (EIS) spectra of the amorphous Ni-C electrodes before and after electrochemical activation, and the Ni-C electrodes after activation with 5000 cycles are shown in Fig. 5a. It can be observed that the impedance spectrum consists of a partial semicircle and an inclined line along the imaginary axis, representing the high frequency and low-frequency components, respectively. The value of the internal resistance (R_b), which includes the sum of the resistance of the electrolyte and the intrinsic resistance of the electrode, can be extracted from the data. Using the ZSimpWin software (Princeton Applied Research, Oak Ridge, TN, USA), the R_b values of the Ni-C electrodes before and

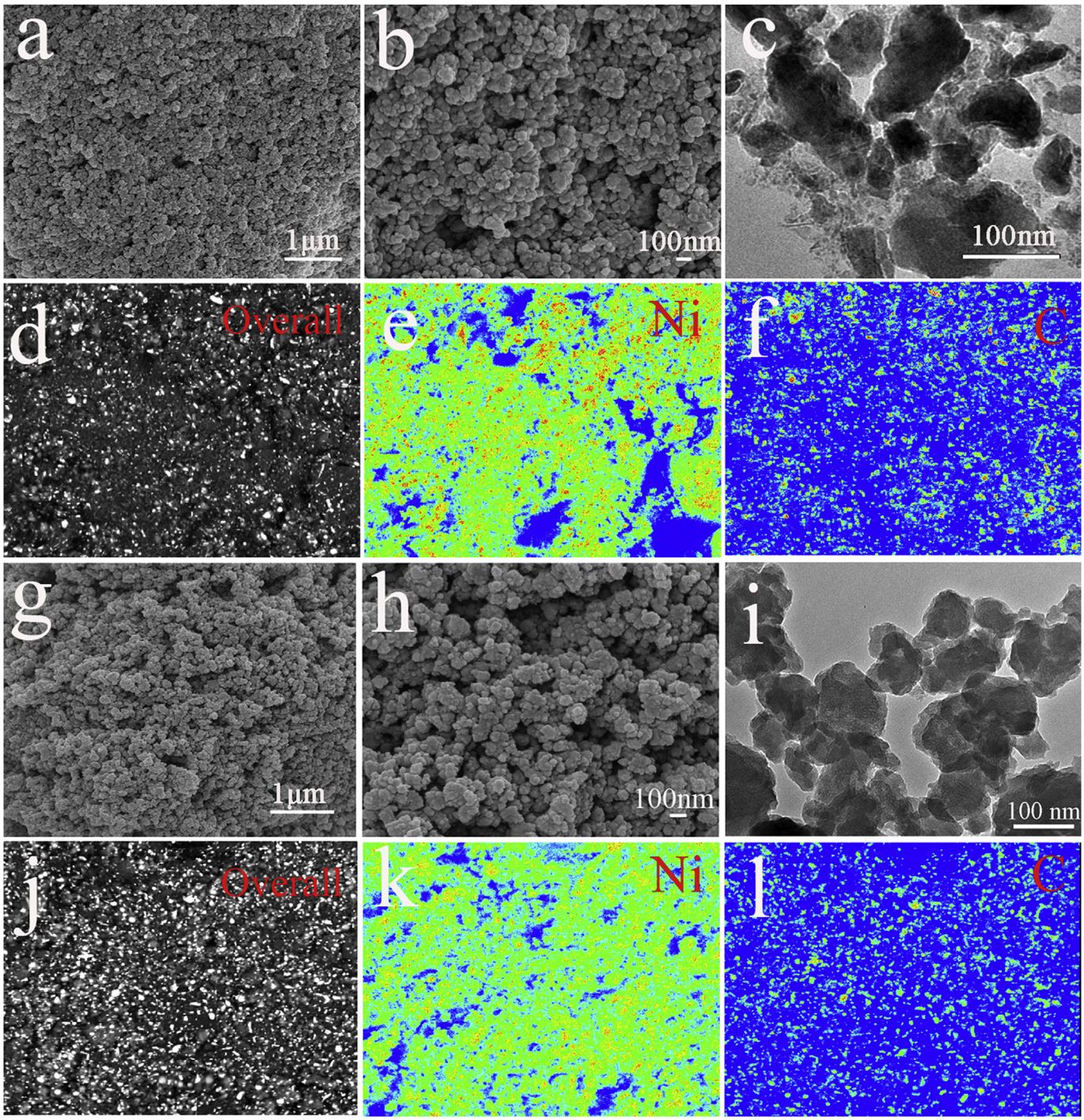

Fig. 2. The microstructure of the Ni-C electrode and the activated Ni-C electrode. (a, b, g, h) SEM patterns of the Ni-C electrode and the activated Ni-C electrode, (c, i) TEM patterns of the Ni-C electrode and the activated Ni-C electrode, and (d, e, f, j, k, l) EDS mapping images of the Ni-C electrode and the activated Ni-C electrode.

after electrochemical activation and after activation for 5000 cycles are 0.601 Ω, 1.015 Ω and 1.738 Ω, respectively, showing that the electrode after electrochemical activation displays a higher R_b than before electrochemical activation. In addition, the conductivity was measured using the four-probe method, and the conductivity values of amorphous Ni-C electrodes before and after electrochemical activation were found to be 0.40 S cm^{-1} and 0.42 S cm^{-1}, respectively. The data for the cycle stability of the Ni-C electrode used as a parameter for further examination of the electrochemical performances are shown in Fig. 5c. It is found that Ni-C electrode shows excellent cycle stability coupled with 95% specific capacitance retention after approximately 5000 cycles.

CV curves with various potential windows were used to evaluate the applicable operation voltage window of the AC//Ni-C asymmetric supercapacitor, as shown in Fig. 6a. When the operation voltage window is lower than 1.6 V, the shape of the CV curve is not fully revealed. By increasing the potential window to more than 1.6 V, other distinct redox peaks emerge in CV curves, suggesting deeper redox reactions on the surface of the Ni-C and AC electrodes. The results indicates that the AC//Ni-C supercapacitor shows the

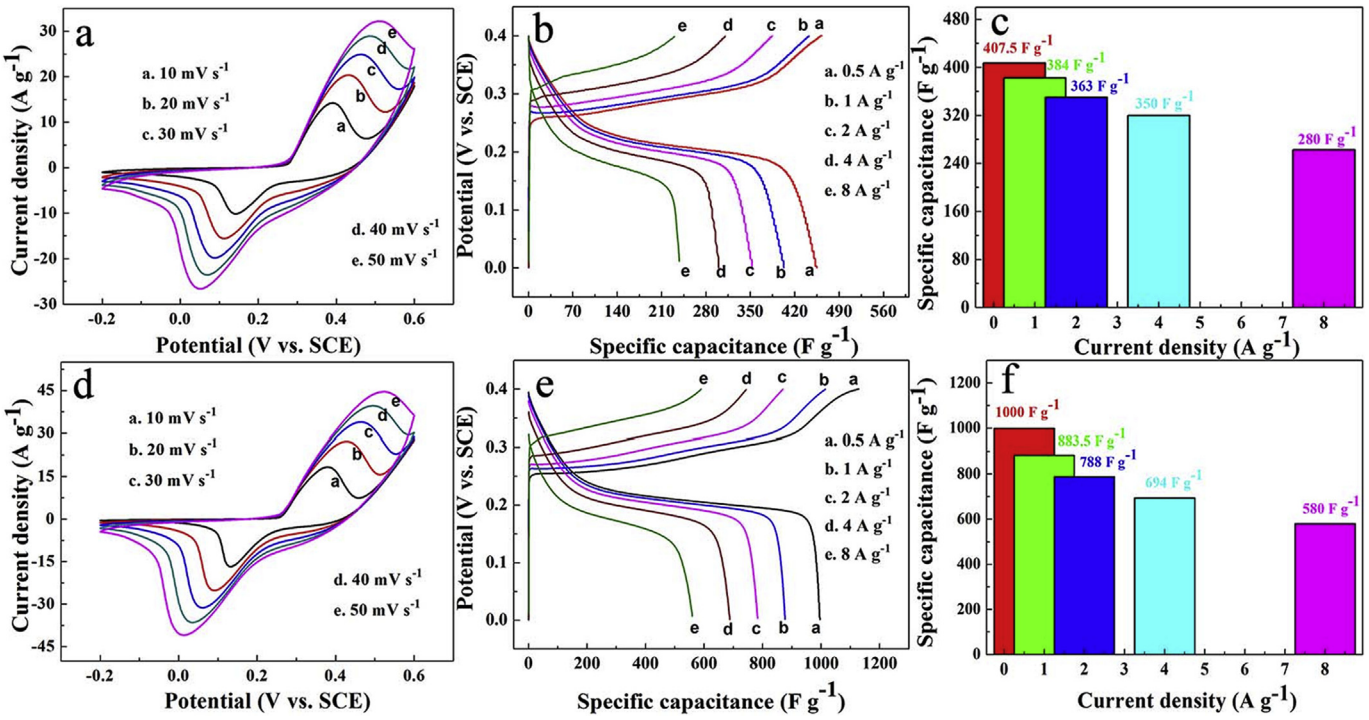

Fig. 3. Electrochemical performances of amorphous Ni-C. (a) CV curves of the Ni-C, (b) GCD curves of Ni-C at different current densities, and (c) C_m of Ni-C electrode at different current densities before electrochemical activation. (d) CV curves of the Ni-C, (e) GCD curves of Ni-C at different current densities, and (f) C_m of Ni-C electrode at different current densities after electrochemical activation.

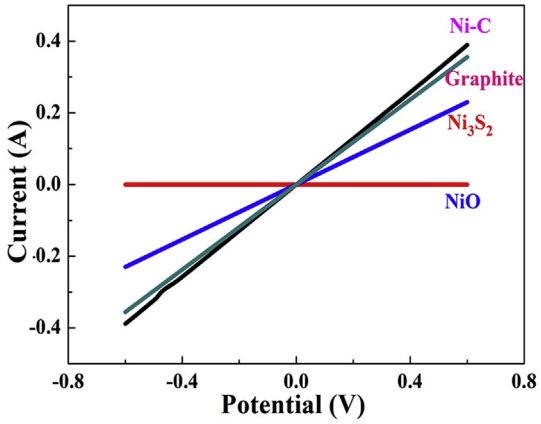

Fig. 4. *I–V* curves of Ni-C, NiO, Ni_3S_2, and graphite.

maximum specific capacitance within the 0–1.6 V potential window. It can be seen from Fig. 6b that the AC//Ni-C exhibits a wide redox peak in the certain potential windows, and the CV curves retain the same shape at higher scan rates, which proving the fast charge-discharge phenomenon of the asymmetric supercapacitor. Fig. 6c shows the constant current charge/discharge profiles and the calculated specific capacitance as a function of the discharge current density is plotted in Fig. 6d. Based on the total mass of the active materials on the positive and negative electrodes, the highest capacitance of 111.9 F g^{-1} is obtained at 0.5 A g^{-1}. The preliminary specific capacitance of the asymmetric supercapacitor is maintained at 71.9 F g^{-1} even for tenfold increase in the current density to 5 A g^{-1} (Fig. 6d), suggesting its excellent rate performance. The Ragone plots of the AC//Ni-C compared to the AC//AC symmetric supercapacitor and other reported capacitors are shown in Fig. 6e. It is obvious that the commercial capacitor and other reported capacitors have a lower energy density than the AC//Ni-C asymmetric supercapacitor. Due to the specific capacitance of the AC//Ni-C, the energy density (E, in Wh kg^{-1}) and power density (P, in W kg^{-1}) can be calculated according to $E = \frac{1}{2}C_m \cdot \Delta V^2$ and $P = \frac{E}{\Delta t}(\Delta t\ (s))$ is the discharge time, ΔV (V) is the potential window, and C_m (F g^{-1}) is the specific capacitance), respectively. The maximum energy density of 39.8 Wh kg^{-1} was obtained at the power density of 400.4 W kg^{-1}, and the energy density of 25.6 Wh kg^{-1} was retained at a power density of 4007 W kg^{-1} for the AC//Ni-C. By comparison, the highest energy density of AC//AC is 5 Wh kg^{-1} at a power density obtained for 158 W kg^{-1}. Furthermore, the energy density of AC//Ni-C is much higher than some of the previously reported supercapacitors, such as hierarchical $NiCo_2S_4$ nanotube@$NiCo_2S_4$ nanosheet arrays on Ni foam//RGO [39], $Ni_2P_2O_7$//graphene [40], and AC//NiO-$Co_3(VO_4)_2$ [41], $NH_4CoPO_4 \cdot H_2O$ microbundles–graphene nanosheets [42], so this supercapacitor can be expected gain a foothold in the traditional EDLCs and Li-ion batteries market. Finally, the long-term cycling stability was also tested by continuous charge-discharge texts at 1 A g^{-1}, and it was found that the AC//Ni-C retains 87% of the specific capacitance after 2000 cycles, demonstrating the excellent performance of the asymmetric supercapacitor (Fig. 6f).

5. Conclusions

In summary, amorphous Ni-C nanoparticles with high electric conductivity and high specific capacitance have been prepared by mechanical alloying method. To the best of our knowledge, this is the first time that nickel carbide has been used as an electrode material in an energy storage device. The variation of the nickel carbide properties before and after the electrochemical activation is discussed here, and some preliminary conclusions are drawn. First, the structure and the phase state of nickel carbide is maintained

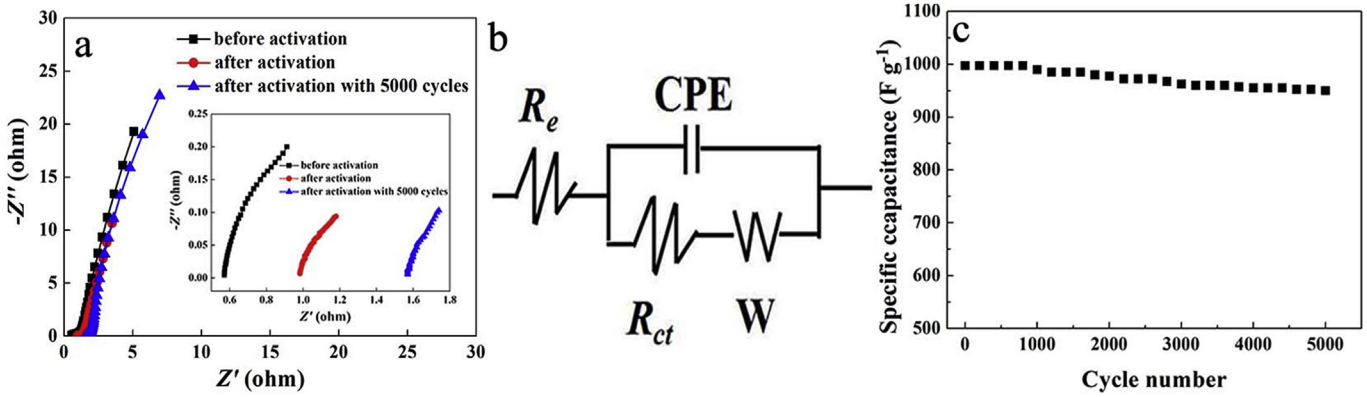

Fig. 5. (a) Electrochemical impedance spectroscopy spectra for the electrode measured before and after electrochemical activation, and the Ni-C electrodes after activation with 5000 cycles (the insets showed the semicircle evident at high-frequency), (b) the corresponding equivalent circuit, (c) the cycle-life of Ni-C.

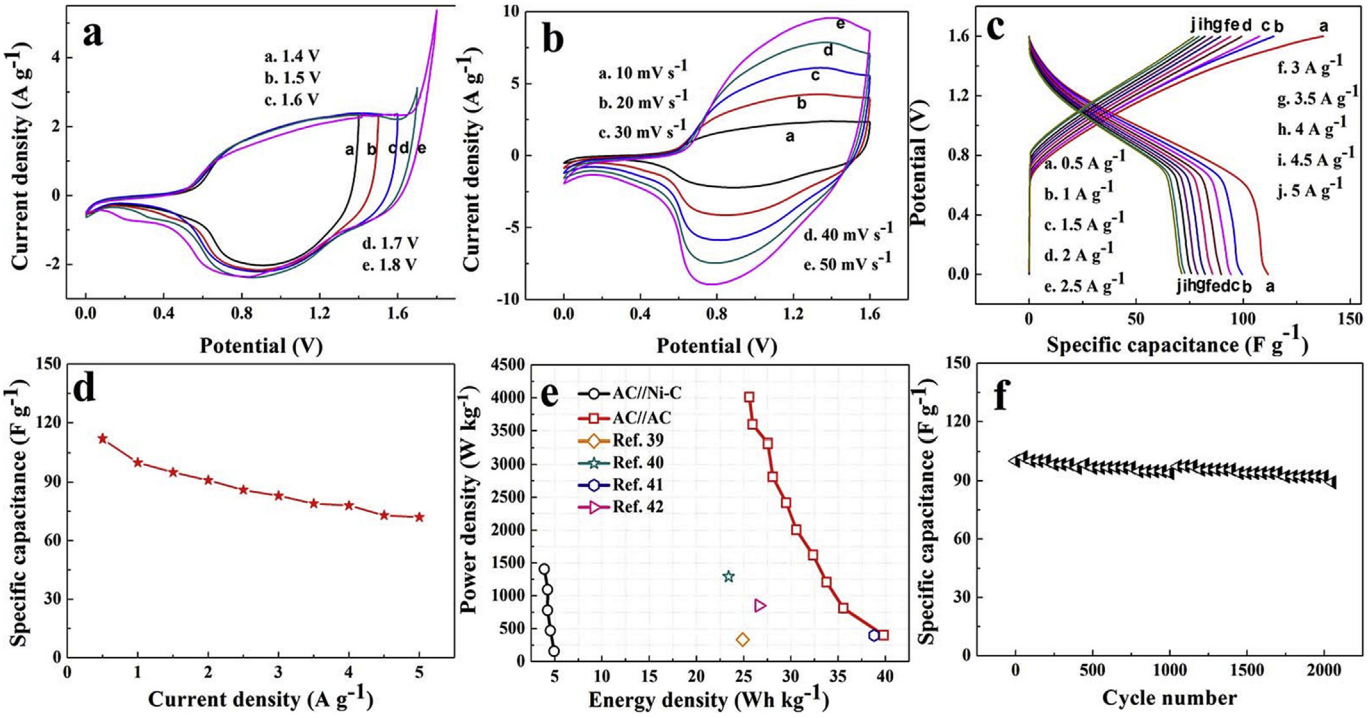

Fig. 6. Electrochemical characterizations of AC//Ni-C asymmetric supercapacitor. (a) CV curves with different operation voltage windows at 10 mV s^{-1}. (b) CV curves at different scan rates. (c) GCD curves and (d) C_m at controlled current densities. (e) the Ragone plots of the AC//Ni-C asymmetric supercapacitor compared with AC//AC symmetric supercapacitor and other reported capacitors. (f) cycle-life of AC//Ni-C asymmetric supercapacitor at the current density of 1 A g^{-1}.

during electrode reaction, give it better cycle stability; Second, nickel carbide show high electrical conductivity, giving rise to its excellent rate performance; Third, the change of the capacity for nickel carbide before and after the reaction is mainly caused by the variation of the impedance. The highest specific capacitance of 1000 F g^{-1} was achieved in a three-electrode structure. An asymmetric supercapacitor assembled from amorphous Ni-C and activated carbon (Ni-C//AC) exhibited the maximum energy density of 39.8 Wh kg^{-1} at the power density of 400.4 W kg^{-1}. Furthermore, the asymmetric supercapacitor exhibited excellent rate capability as well as good cycling stability. Thus there is reason to believe that nickel carbide materials will play some role in the field of energy storage devices.

Acknowledgments

This work was supported by the National Natural Science Foundation of China (no. 21403099), the Natural Science Foundation of Gansu Province (no. 1506RJZA107), and the fund of the State Key Laboratory of Advanced Processing and Recycling of Nonferrous Metals, Lanzhou University of Technology (no. SKLAB02014005).

Appendix A. Supplementary data

Supplementary data related to this article can be found at https://doi.org/10.1016/j.matchemphys.2017.11.032.

References

[1] Z.Y. Xiong, C.L. Liao, W.H. Han, X.G. Wang, Mechanically tough large-area hierarchical porous graphene films for high-performance flexible supercapacitor applications, Adv. Mater 27 (2015) 4469–4475.

[2] Z. Zhou, Y.R. Zhu, Z.B. Wu, F. Lu, M.J. Jing, X.B. Ji, Amorphous RuO_2 coated on carbon spheres as excellent electrode materials for supercapacitors, RSC Adv. 4 (2014) 6927–6932.

[3] D. Chen, Q.F. Wang, R.M. Wang, G.Z. Shen, Ternary oxide nanostructured materials for supercapacitors: a review, J. Mater. Chem. A 3 (2015) 10158–10173.

[4] H.C. Chen, S. Chen, M.Q. Fan, C. Li, D. Chen, G.L. Tian, K.Y. Shu, Bimetallic nickel cobalt selenides: a new kind of electroactive material for high-power energy storage, J. Mater. Chem. A 3 (2015) 23653–23659.

[5] D.P. Dubal, D. Aradilla, G. Bidan, P. Gentile, T.J.S. Schubert, J. Wimberg, S. Sadki, P.G. Romero, 3D hierarchical assembly of ultrathin MnO_2 nanoflakes on silicon nanowires for high performance micro-supercapacitors in Li-doped ionic liquid, Sci. Rep. 5 (2015) 9771–9781.

[6] X.L. Dong, Z.Y. Guo, Y.F. Song, M.Y. Hou, J.Q. Wang, Y.G. Wang, Y.Y. Xia, Flexible and wire-shaped micro-supercapacitor based on $Ni(OH)_2$-nanowire and ordered mesoporous carbon electrodes, Adv. Funct. Mater 24 (2014) 3405–3412.

[7] D. Chakravarty, D.J. Late, Microwave and hydrothermal syntheses of WSe_2 micro/nanorods and their application in supercapacitors, RSC Adv. 5 (2015) 21700–21709.

[8] Q. Zhang, Y.H. Deng, Z.H. Hu, Y.F. Liu, M.M. Yao, P.P. Liu, Seaurchin-like hierarchical $NiCo_2O_4$@$NiMoO_4$ core-shell nanomaterials for high performance supercapacitors, Phys. Chem. Chem. Phys. 16 (2014) 23451–23460.

[9] L.F. Chen, Z.H. Huang, H.W. Liang, Q.F. Guan, S.H. Yu, Bacterial-cellulose-derived carbon nanofiber@MnO_2 and nitrogen-doped carbon nanofiber electrode materials: an asymmetric supercapacitor with high energy and power density, Adv. Mater 25 (2013) 4746–4752.

[10] R. Li, S.L. Wang, J.P. Wang, Z.H. Huang, Ni_3S_2@CoS cor-shell nano-triangular pyramid arrays on Ni foam for high-performance supercapacitors, Phys. Chem. Chem. Phys. 17 (2015) 16434–16442.

[11] F.H. Su, X.M. Lv, M.H. Miao, High-performance two-ply yarn supercapacitors based on carbon nanotube yarns dotted with Co_3O_4 and NiO nanoparticles, Small 11 (2015) 854–861.

[12] L.Y. Niu, Z.P. Li, Y. Xu, J.F. Sun, W. Hong, X.H. Liu, J.Q. Wang, S.R. Yang, Simple synthesis of amorphous $NiWO_4$ nanostructure and its application as a novel cathode material for asymmetric supercapacitors, ACS Appl. Mater. Interfaces 5 (2013) 8044–8052.

[13] X.H. Lu, Y.X. Zeng, M.H. Yu, T. Zhai, C.L. Liang, S.L. Xie, M.S. Balogun, Y.X. Tong, Oxygen-deficient hematite nanorods as high-performance and novel negative electrodes for flexible asymmetric supercapacitors, Adv. Mater 26 (2014) 3148–3155.

[14] D. Ghosh, S. Giri, M. Moniruzzaman, T. Basu, M. Mandal, C.K. Das, α- $MnMoO_4$/graphene hybrid composite: high energy density supercapacitor electrode material, Dalton Trans. 43 (2014) 11067–11076.

[15] R.T. Wang, X.B. Yan, Superior asymmetric supercapacitor based on Ni-Co oxide nanosheets and carbon nanorods, Sci. Rep. 4 (2014) 3712–3721.

[16] V. Augustyn, P. Simonbc, B. Dunn, Pseudocapacitive oxide materials for high-rate electrochemical energy storage, Energy Environ. Sci. 7 (2014) 1597–1614.

[17] H. Pang, Y.Z. Zhang, W.Y. Lai, Z. Hu, W. Huang, Lamellar $K_2Co_3(P_2O_7)_2 \cdot 2H_2O$ nanocrystal whiskers: high-performance flexible all-solid-state asymmetric micro-supercapacitors via inkjet printing, Nano Energy 15 (2015) 303–312.

[18] Y. Zhang, M. Park, H.Y. Kim, S.J. Park, Moderated surface defects of Ni particles encapsulated with NiO nanofibers as supercapacitor with high capacitance and energy density, J. Colloid Interface Sci. 500 (2017) 155–163.

[19] Y. Zhang, S.J. Park, Incorporation of RuO2 into charcoal-derived carbon with controllable microporosity by CO2 activation for high-performance supercapacitor, Carbon 122 (2017) 287–297.

[20] G.F. Cai, X. Wang, M.Q. Cui, P. Darmawan, J.X. Wang, Electrochromo-supercapacitor based on direct growth of NiO nanoparticles, Nano Energy 12 (2015) 258–267.

[21] F. Cao, G.X. Pan, X.H. Xia, P.S. Tang, H.F. Chen, Synthesis of hierarchical porous NiO nanotube arrays for supercapacitor application, J. Power Sources 264 (2014) 161–167.

[22] C. Guan, Y.D. Wang, Y.T. Hu, J.L. Liu, K.H. Ho, W. Zhao, Z.X. Fan, Z.X. Shen, H. Zhang, J. Wang, Conformally deposited NiO on a hierarchical carbon support for high-power and durable asymmetric supercapacitors, J. Mater. Chem. A 3 (2015) 23283–23288.

[23] J.Q. Yang, X.H. Duan, W. Guo, D. Li, H.L. Zhang, W.J. Zheng, Electrochemical performances investigation of NiS/rGO composite as electrode material for supercapacitors, Nano Energy 5 (2014) 74–81.

[24] Y. Yu, W.Y. Gao, Z.X. Shen, Q. Zheng, H. Wu, X. Wang, W.G. Song, K.J. Ding, A novel Ni_3N/graphene nanocomposite as supercapacitor electrode material with high capacitance and energy density, J. Mater. Chem. A 3 (2015) 16633–16641.

[25] Z. Zhang, Z.Y. Huang, L. Ren, Y.Z. Shen, X. Qi, J.X. Zhong, One-pot synthesis of hierarchically nanostructured Ni_3S_2 dendrites as active materials for supercapacitors, Electrochim. Acta 149 (2014) 316–323.

[26] X.H. Xia, Y.Q. Zhang, D.L. Chao, Q.Q. Xiong, Z.X. Fan, X.L. Tong, J.P. Tu, H. Zhang, H.J. Fan, Tubular TiC fibre nanostructures as supercapacitor electrode materials with stable cycling life and wide-temperature performance, Energy Environ. Sci. 8 (2015) 1559–1568.

[27] M. Ghidiu, M.R. Lukatskaya, M.Q. Zhao, Y. Gogotsi, M.W. Barsoum, Conductive two-dimensional titanium carbide'clay'with high volumetric capacitance, Nature 516 (2014) 78–81.

[28] M. Naguib, M. Kurtoglu, V. Presser, J. Lu, J.J. Niu, M. Heon, L. Hultman, Y. Gogotsi, M.W. Barsoum, Two-dimensional nanocrystals produced by exfoliation of Ti_3AlC_2, Adv. Mater 23 (2011) 4248–4253.

[29] D. Wang, L.B. Kong, M.C. Liu, W.B. Zhang, Y.C. Luo, L. Kang, Amorphous Ni-P materials for high performance pseudocapacitors, J. Power Sources 274 (2015) 1107–1113.

[30] Y.Z. Su, K. Xiao, N. Li, Z.Q. Liu, S.Z. Qiao, Amorphous $Ni(OH)_2$@ three-dimensional Ni cor-shell nanostructures for high capacitance pseudocapacitors and asymmetric supercapacitors, J. Mater. Chem. A 2 (2014) 13845–13853.

[31] S.S. Zhu, Y.M. Dai, W. Huang, C.X. Zhang, Y.Q. Zhao, L.H. Tan, Z.Z. Wang, In situ preparation of NiO nanoflakes on Ni foams for high performance supercapacitors, Mater. Lett. 161 (2015) 731–734.

[32] K. Yan, L.B. Kong, Y.H. Dai, M. Shi, K.W. Shen, B. Hu, Y.C. Luo, L. Kang, Design and preparation of highly structure-controllable mesoporous carbons at the molecular level and their application as electrode materials for supercapacitors, J. Mater. Chem. A 3 (2015) 22781–22793.

[33] Y. Zhang, M. Park, H.Y. Kim, B. Ding, S.J. Park, In-situ synthesis of nanofibers with various ratios of BiOClx/BiOBry/BiOIz for effective trichloroethylene photocatalytic degradation, Appl. Surf. Sci. 384 (2016) 192–199.

[34] Y. Zhang, M. Park, H.Y. Kim, S.J. Park, In-situ synthesis of graphene oxide/BiOCl heterostructured nanofibers for visible-light photocatalytic investigation, J. Alloy Compd. 686 (2016) 106–114.

[35] L.P. Sui, S.H. Tang, Z. Dai, Z.T. Zhu, H.X. Huangfu, X.L. Qin, Y.X. Deng, G.M. Haarberg, Supercapacitive behavior of an asymmetric supercapacitor based on a $Ni(OH)_2$/XC-72 composite, New J. Chem. 39 (2015) 9363–9371.

[36] S.I. Kim, J.S. Lee, H.J. Ahn, H.K. Song, J.H. Jang, Facile route to an efficient NiO supercapacitor with a three-dimensional nanonetwork morphology, ACS Appl. Mater. Interfaces 5 (2013) 1596–1603.

[37] C.J. Zhao, Z.M. Zhang, Q. Wang, S.D. Min, X.Z. Qian, Vertically oriented Ni_3S_2/RGO/Ni_3S_2 nanosheets on Ni foam for superior supercapacitors, RSC Adv. 5 (2015) 63528–63536.

[38] Y.Z. Jiang, Z.H. Li, B.B. Li, J.Y. Zhang, C.M. Niu, Ni_3Si_2 nanowires grown in situ on Ni foam for high-performance supercapacitors, J. Power Sources 320 (2016) 13–19.

[39] H.C. Chen, S. Chen, H.Y. Shao, C. Li, M.Q. Fan, D. Chen, G.L. Tian, K.Y. Shu, Hierarchical $NiCo_2S_4$ nanotube@$NiCo_2S_4$ nanosheet arrays on Ni foam for high-performance supercapacitors, Chem. Asian J. 11 (2016) 248–256.

[40] C.Z. Wei, C. Cheng, S.S. Wang, Y.Z. Xu, J.D. Wang, H. Pang, Sodium-doped mesoporous $Ni_2P_2O_7$ hexagonal tablets for high-performance flexible all-solid-state hybrid supercapacitors, Chem. Asian J. 10 (2015) 1731–1737.

[41] W.B. Zhang, L.B. Kong, X.J. Ma, Y.C. Luo, L. Kang, Three-dimensional nanostructured NiO-$Co_3(VO_4)_2$ compound on nickel foam as pseudocapacitive electrodes for electrochemical capacitors, J. Alloy. Compd. 627 (2015) 313–319.

[42] S.M. Wang, H. Pang, S.S. Zhao, W.F. Shao, N.N. Zhang, J.S. Zhang, J. Chen, S.J. Li, $NH_4CoPO_4 \cdot H_2O$ microbundles consisting of one-dimensional layered microrods for high performance supercapacitors, RSC Adv. 4 (2014) 340–347.